H and CO Co-induced Adatom Formation on Cu in CO_2 Electroreduction Conditions

Zisheng Zhang,[a] Winston Gee,[a] Philippe Sautet,[a,b,c,*] Anastassia N. Alexandrova[a,c,d,*]

[a] Department of Chemistry and Biochemistry, [b] Department of Chemical and Biomolecular Engineering, [c] California NanoSystems Institute, [d] Department of Materials Science and Engineering, University of California, Los Angeles, CA 90094, USA

ABSTRACT

Dynamic restructuring of Cu electrode has been observed under electrochemical conditions, and it has been hypothesized to underly the unique reactivity of Cu towards CO_2 electroreduction. Surface roughening is one of the key surface phenomena to Cu activation, in which the surface forms numerous atomic vacancies and adatoms. However, the atomic structure of such surface motifs, in the presence of relevant adsorbates has remained elusive. Here, we explore the chemical space of Cu surface restructuring under coverage of CO and H in realistic electroreduction conditions, by a combination of grand canonical density functional theory and global optimization techniques, from which we construct a potential-dependent grand canonical ensemble representation of the surface. Significant vertical displacement of surface Cu atoms is observed in the regime of intermediate and mixed CO and H coverage. This regime, while predicted to be thermodynamically inaccessible, is kinetically controlled, presenting a tough challenge for theory. To investigate the kinetic trapping effects, we develop a quasi-kinetic Monte Carlo simulation to track the evolution of the system during a simulated cathodic scan. The simulation reveals the path that the system takes across the coverage space and the metastable structures that the system evolves into along the way. Chemical bonding analysis is performed on the metastable structures with elevated Cu*CO species to understand its formation mechanism. By molecular dynamics simulations and free energy calculations, the surface chemistry of the Cu*CO species is explored, and we identifies potential mechanisms via which the Cu*CO species may diffuse or dimerize. This work provides rich atomistic insights into the surface roughening phenomenon and the structure of the involved species. It also features generalizable methods to explore the chemical space of restructuring surfaces with mixed adsorbates, and its evolution in non-equilibrium.

TOC GRAPHICS

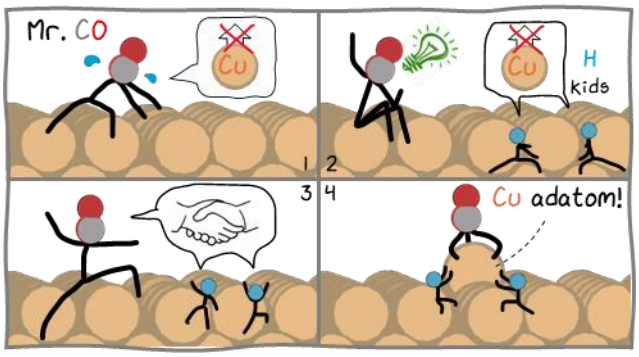

INTRODUCTION

In the quest for a sustainable future, electrocatalysis stands as a cornerstone, driving the electrochemical storage of renewable energy and paving the way for the production of valuable molecules from waste and greenhouse gases. Knowledge of the surface structure under reaction conditions is central to electrocatalyst development, as it is the prerequisite to mechanistic investigation and subsequent optimization. However, the more we know, the more we realize we don't know -- as the resolution of surface characterization techniques advances in recent years, it becomes increasingly evident that the electrocatalytic surfaces are not static landscapes. Instead, they are dynamic arenas where an ensemble of catalyst states fight in chaos, with a diverse distribution of geometry, composition, and reactivity.[1,2]

Copper, the only transition metal that efficiently catalyzes CO_2 reduction reaction (CO_2RR) into deeper C_{2+} reduction products,[3] is intriguingly notorious for undergoing complex redox and structural dynamics under electrochemical conditions.[4,5] From bulk phase transition to surface reconstruction,[6] and from dissolution-redeposition to nanoclustering,[7,8] the fluxional nature of Cu electrocatalysts seem to underpin their unique reactivity. A key surface species to the above mentioned phenomena is the Cu adatom, whose existence has been confirmed in CO_2RR and CO electro-oxidation conditions.[9,10] Multiple structural models of the adatom have been proposed, but most of them were built based on experimental signals and speculations, or neglected the many realistic aspects.[9,11,12] The atomic structure and formation mechanisms of these surface adatoms, under the effect of electrode potential and surface adsorbates, is still lacking.

As a sequel to our previous efforts to understand the H-induced restructuring of Cu(100)[13] and Cu(111)[14] in electroreduction conditions, here we investigate the case where the surface is under a mixed coverage of both *H and *CO, which is more relevant to CO_2RR and CO electro-oxidation reactions. By performing grand canonical

genetic algorithm (GCGA) global optimization and grand canonical density functional theory (GCDFT) calculation, we constructed potential-dependent grand canonical ensemble and free energy landscapes of Cu surfaces under different coverages of *H and *CO. Due to the failure of Boltzmann statistics in predicting any changes to the Cu surface morphology, we devised a pseudo-kinetic Monte Carlo simulation to address the non-equilibrium nature of the system and to identify the metastable states that the system would be trapped into under reducing potentials. A number of Cu*CO species, which are elevated from the top surface under the co-influence of atop *CO and surrounding *H, were predicted to form in the CO_2RR-relevant potential regime. Chemical bonding origin of the H and CO co-induced adatom formation is investigated, and the possible pathways for surface migration and dimerization of the formed adatoms are probed by free energy calculations. This study provides rich insights into the formation and chemistries of the roughened Cu surfaces in realistic electrochemical conditions, which can benefit the electrocatalysis community in mechanistic investigations and further optimization of Cu electrocatalysts.

RESULTS & DISCUSSION

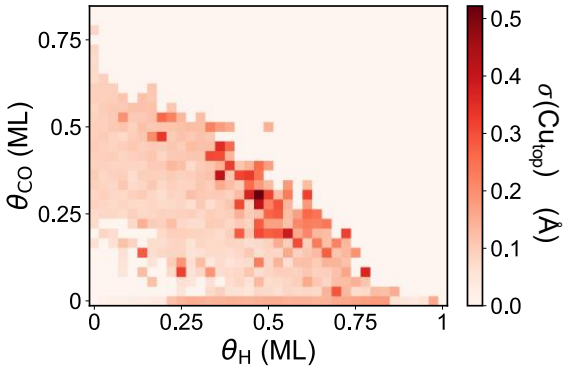

Figure 1. Vertical displacement of surface Cu atoms as a function of CO and H coverages, for the global minimum structure of each coverage state, without applied potential. Darker color indicates a larger standard deviation in heights of top surface Cu atoms.

We consider the Cu surfaces to be under the coverage of both CO and H, which are the two main reaction intermediates in CO_2RR in near-neutral or acidic conditions. Due to the extremely large chemical space spanned by surface rearrangement and mixed adsorbate coverage, grand canonical genetic algorithm(GCGA)[13,15–17] is used to globally optimize the configuration of Cu(100), (111), and (711) step under the coverage of both H and CO (Methods and Supplementary Note 1 for details). To be specific, the system is allowed to exchange H and CO with a reservoir with fixed chemical potentials of H and CO (μ_H and μ_{CO}), so that the search direction in the compositional space will be self-adaptive. To cover the chemically relevant range of μ_H and μ_{CO}, multiple GCGA searches are performed at a pH of 7, CO partial pressure of 1 atm, and electrode potentials between 0 and -1 V_{SHE}.

In total, 16,830, 22,511, and 20,555 unique catalyst states are obtained for Cu(100), Cu(111), and Cu(711), respectively. The main body of this work will be focusing on the reconstruction of Cu(100), which has well-studied H-induced restructuring and chemistry

in a previous work, while the other shares similar behaviors (Figure S2). All of the three collections well cover the regime of mixed H and CO adsorption between 1 ML H and 0.75 ML CO, with a quite broad distribution of geometries. Figure 1 shows the standard deviation of top surface Cu atoms' heights as a function of H coverage and CO coverage, which represents the extent of structural rearrangement on the top monolayer of the surface. Under the coverage of only CO, the Cu surface stays in the pristine (100) configuration. Under coverage of only H, shifted-row configurations can form only at higher H coverages, which is consistent with our previous findings.[13] Neither H-only, nor CO-only coverage can induce any adatom formation at a constant surface density of Cu.[14] However, at an intermediate coverage of both H and CO, many catalyst states with adatoms become accessible. This can be seen from the much larger standard deviations of Cu (reaching 0.5 Å), in the region with CO coverage from 0.2 to 0.5 ML and H coverage from 0.3 to 0.7 ML.

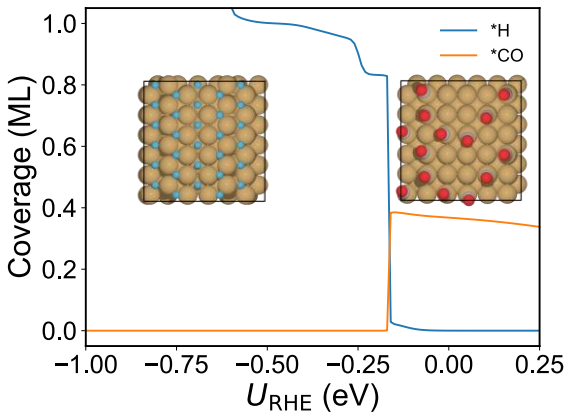

Figure 2. CO and H coverage as functions of electrochemical potential from Boltzmann statistics. Representative structure of H-only and CO-only coverage structures are shown as insets.

To assess the relative accessibility of the identified structures under the applied bias, we performed grand canonical density functional theory (GCDFT) calculations on the low-energy local minima (LELM) for each adsorbate coverage to construct a grand canonical ensemble of H, CO, and electrons. This approach makes possible a comparison of potential-dependent thermodynamic stability for the states in the ensemble, according to grand canonical free energetics. To study the evolution of the surface structure under varying electrochemical potentials, we first apply Boltzmann statistics to calculate the population of the states in the ensemble, solely based on thermodynamics (Figure 2). The surface Cu arrangement is predicted to stay pristine near zero applied potential with CO coverage of about 0.4 ML and no H. It rearranges into the doubly shifted-row configuration at more negative potentials with H coverage of about 1 ML and no CO. However, the jump in adsorbate coverage from CO-only to H-only states is abrupt – the transition is d-function like, and occurs within a very narrow potential window, skipping all mixed coverage states. From the point of view of the mechanism of surface reconstruction and its dynamics, this abrupt changes appears rather unphysical.

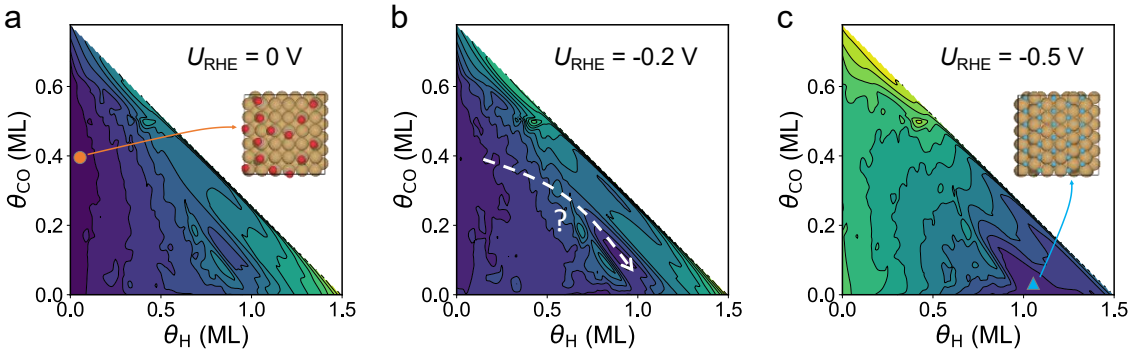

Figure 3. Grand canonical free energy surfaces as functions of H and CO coverages, at electrochemical potentials of (a) 0 V, (b) -0.2 V, and (c) -0.5 V, in RHE scale. Dark blue and light yellow colors represent low and high free energies, respectively.

The unphysical "coverage jump" behaviour in the thermodynamic picture prompt us to look into the detailed evolution of the free energy landscape in the coverage space. At 0 V_{RHE}, the global minimum (GM) and LELMs all lie in the region corresponding to CO-only coverage. As the potential shifts to -0.2 V_{RHE}, the region of low CO coverage and high H coverage becomes as thermodynamically competitive as the CO-only region. At -0.5 V_{RHE}, the H-only region becomes the GM. The "coverage jump" corresponds to a critical electrochemical potential where the high H coverage states tie with the high CO coverage states. After a tiny increment of reducing potential, the high H coverage states outcompete the high CO coverage states in terms of free energy and become the new GM. As a result, the thermodynamic-only picture would predict a sudden inversion of H and CO coverages on the surface. However, in reality, changes in coverage should be continuous and differential, with the surface gaining, losing, or displacing one or few adsorbate(s) at a time, rather than all at once. In other words, when the system is traversing the free energy landscape, its moves are kinetically limited to neighboring coverage states, making it a non-equilibrium and undermining the Boltzmann statistics (which would be achievable at infinitely long times). When the system evolves from the initial GM (CO-only coverage) to the new GM (H-only coverage), it is bound to visit a series of coverage states along the way. Such progression can be kinetically hindered due to the bumpy and multi-minima nature of the free energy landscape, causing the system to be stranded, and even trapped, in a relatively flat metastable regime of mixed coverage of H and CO.

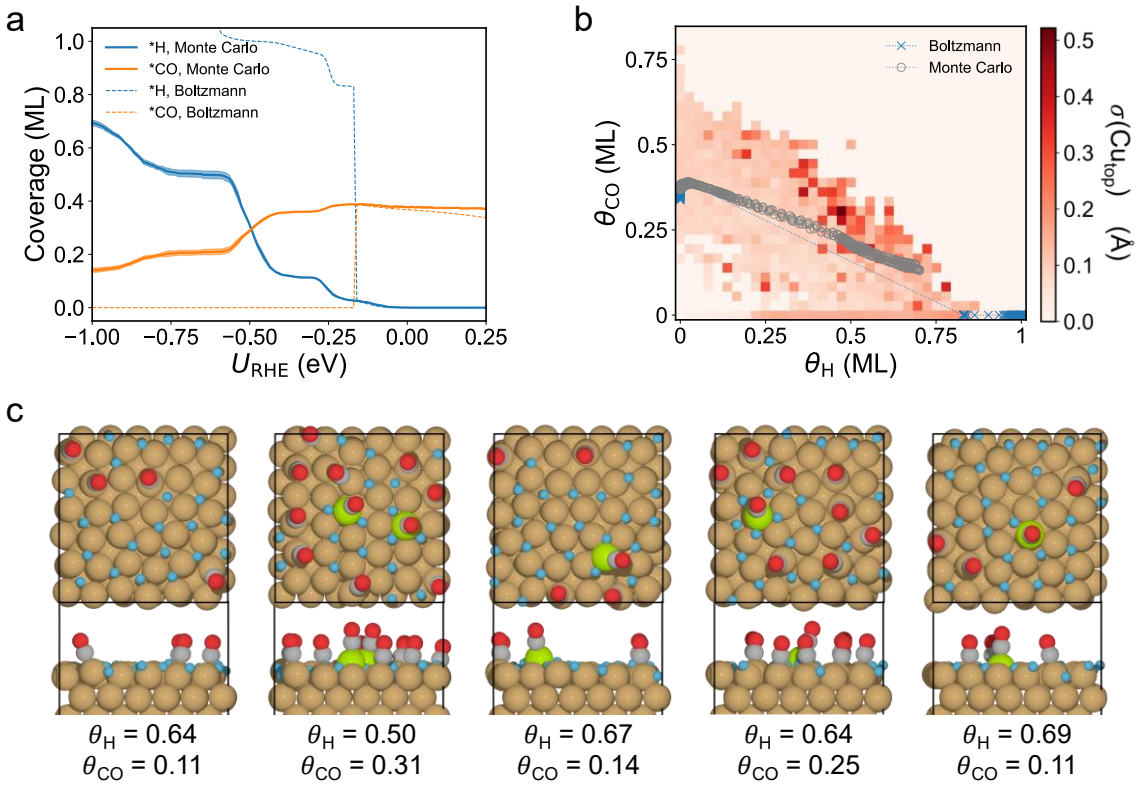

Figure 4. Quasi-kinetic Monte Carlo simulations of surface structure and coverage evolution. (a) H and CO coverages as functions of electrochemical potential, from Boltzmann statistics (dashed lines) and Monte Carlo simulations (solid lines). (b) Evolution of the system's coverage state on the vertical displacement map of surface atoms, with respected to H and CO coverages, during a simulated cathodic scan, from Boltzmann statistics (as blue crosses) and Monte Carlo simulations (as red circles). (c) Notable structures (with a maximum population of at least 10%) with significant surface Cu rearrangements under mixed coverage of H and CO. Color code: Cu – brown; H – blue; C – grey; O – red; elevated Cu – green.

To identify the states that the system would visit along the way in the coverage space, we devise a quasi-kinetic Monte Carlo (MC) simulation to investigate the surface changes under varying electrochemical potential. The surface is represented by a 10×10 lattice of the cells (each with the same size as in GCGA sampling, i.e. a total of 60×60 surface model). Two types of moves are considered to represent the electrolyte-electrode and intra-electrode exchange of adsorbates: (i) desorb or adsorb one adsorbate; (ii) displace one adsorbate to a neighboring cell. The kinetic barriers of these moves are assumed to scale with their associated grand canonical free energy changes, which introduces potential dependence and a sense of time into the simulation. During the simulated cathodic scan, the electrode potential is changed in a small increment of 10 mV. At each potential, the system undergoes a finite number of simulation steps (2 million, corresponding to the timescales of microseconds, see Supplementary Note 2), which is sufficient to bring the system to a quasi-equilibrium, but not guaranteeing it to reach the global minima.

The MC simulation presents a completely different picture from the thermodynamic one. The majority adsorbate in the beginning, CO, will still be replaced by H as the potential scans to more negative, but the onset of such crossover is at a much more negative potential (about 0.2 V_{RHE} for Boltzmann; about 0.5 V_{RHE} for MC), and the transition is much smoother than in the thermodynamic-only picture (Figure 4a). Even at very negative potentials, the system never goes into the H-only coverage state, suggesting trapping in a metastable LM regime without reaching the GM.

The path in the coverage space, as the system traverses the potential-dependent free energy landscape, is plotted on the structural deviation map (as in Figure 1) in Figure 4b. The Boltzmann picture predicts an abrupt jump from CO-only to H-only coverage, whereas MC predicts a smooth, continuous path from CO-only coverage into the region of roughly 0.2 ML CO coverage and 0.6 ML H coverage.

More interestingly, the observed regime of mixed coverage coincides with the production of Cu adatoms on the surface (Figure 4c). By tracking the statistics of states in the Monte Carlo simulations, we could obtain the population of each state in the metastable regime during the simulated cathodic scan (Figure S4). Starting at about -0.45 V_{RHE}, there is a significant replacement of CO by H on the surface, leading to a p4g-like surface arrangement of Cu. In the range of -0.5 to -0.7 V_{RHE}, multiple catalyst states with Cu*CO adatoms gain population up to 30%, which are shown in Figure 4c and ordered by onset potential (from positive to negative). The arrangement of surface Cu are primarily in the p4g-like configuration, with minority in the shifted-row configuration. The overall population of adatoms peaks (up to about 50%) in the coverage range of 0.50 to 0.64 ML for H and 0.14 to 0.31 for CO. The elevation of the Cu*CO species decreases at a higher H-to-CO coverage ratio, due to the strong stabilization of in-plane Cu configurations at very high H coverage.[13,14]

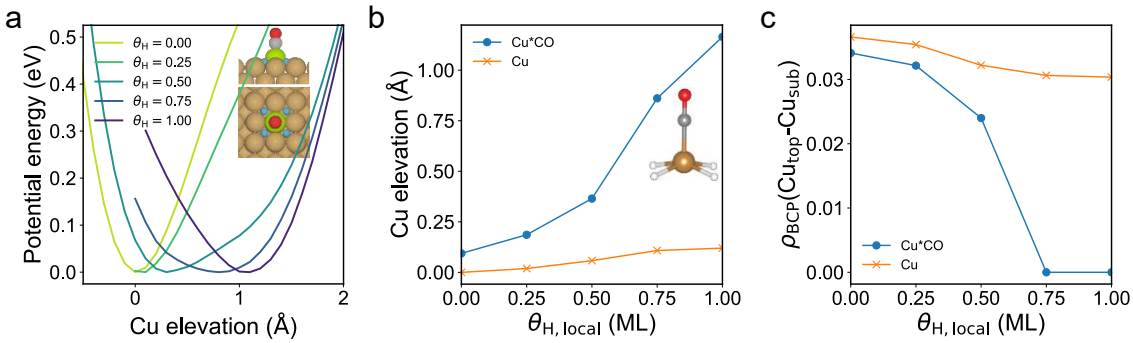

Figure 5. Chemical bonding analysis of the elevated Cu*CO species. (a) Potential energy surface of the Cu elevation with or without atop CO at different local H coverages. (b) Cu elevation in the minima structures with CO (blue) and without CO (orange) at different local H coverages. (c) Electron density at the bond critical points of Cu_{top}-Cu_{sub} bonds with CO (blue) and without CO (orange) at different local H coverages.

We now investigate the electronic structure origin of the formation of elevated Cu*CO species. Due to the complexity and diversity of the local environment of Cu*CO species in the mixed coverage states, we approach it by using a minimal model of pristine Cu(100) with one Cu with or without CO and H adsorbates in different local coverages. We first focus on a top surface Cu with an atop CO and 0 to 4 H surrounding it, corresponding to a local H coverage of 0 to 1 ML. The potential energy surface (PES) of the Cu atom moving in vertical direction out of the surface is obtained by a relaxed scan (Figure 5a). When there is no H in the vicinity of the Cu*CO, the minimum of the PES is at 0.09 Angstrom relative to the bare pristine surface, showing a negligible elevation. The position of the minima and the shape of the PES stays about the same at 0.25 ML local H coverage. As the local H coverage around the Cu*CO further increases, the PES becomes flatter, and the minimum shifts to a higher elevation. At a local H coverage of 0.75 ML, the minimum shifts to a 0.86 Angstrom elevation, and it further increases to 1.17 Å at 1 ML local H coverage, corresponding to formation of the adatom species. Note that this H-induced elevation of top surface Cu is only significant with an atop CO adsorbate – if without CO, the maximal elevation is merely 0.12 Å at 1 ML local H coverage (Figure 5b). In summary, there is not a kinetic barrier associated with the adatom formation on any of the fixed-composition PES's, but rather, the minimum of the PES evolves as the local H coverage increases, naturally bring the Cu*CO to the adatom state at higher local H coverage.

The evolution of the PES shape is also quite intriguing: the PES becomes flatter when local H coverage increases from 0 to 0.75 ML, but it gets steeper again at 1 ML. The coverage-dependent flatness of the PES suggests the presence of two competing interactions, one to hold Cu in-plane and another to drag it out-of-plane. They strike a balance at 0.75 ML local H coverage, marking a critical point for the transition to the adatom state. The adatom formation indeed resembles a phase transition process, which takes place in the local H coverage range of 0.5 to 0.75 ML. This is accompanied by the

breaking of chemical bonds between top surface Cu and subsurface Cu atoms, as quantum theory of atom in molecule (QTAIM) analysis suggests in Figure 5c. Note that H merely acts as a "lubricant" which partially weaken the Cu_{top}-Cu_{sub} bonds.[13] The adatom state with a distorted pyramidal configuration, with electron localization and molecular-like characteristics (Supplementary Note 3), can only be stabilized in the presence of an atop CO adsorbate.

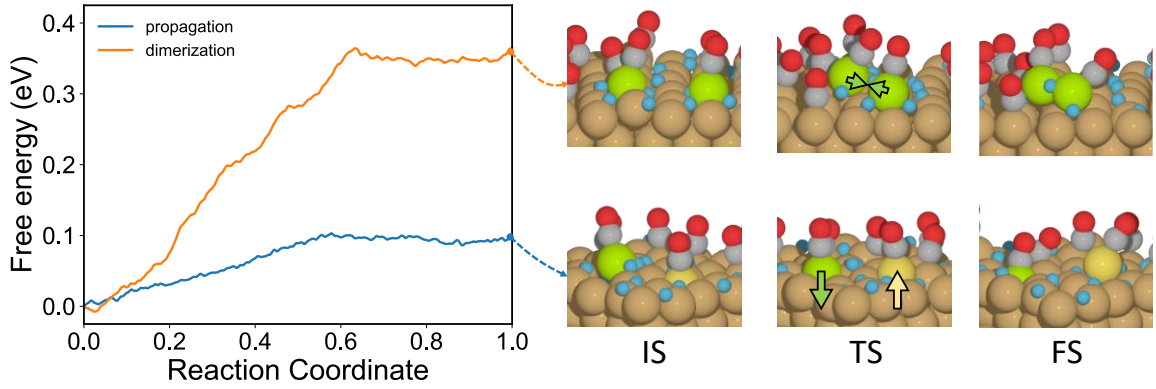

Figure 6. Free energy profiles of Cu*CO propagation and dimerization.

Are the formed Cu*CO species prone to further evolution? Since the H adsorbates are highly mobile, and the Cu_{top}-Cu_{sub} bond strengths depend heavily on the local H coverages, we perform molecular dynamics (MD) simulations on the selected catalyst states in Figure 4. In the timescale of a few picoseconds, the Cu*CO species decorated with co-adsorbed Hs does not move laterally. However, for some Cu*CO species, we observe an unusual and coupled set of motions: the initially-elevated Cu*CO can sink back into the top surface layer, and another in-plane Cu (a second nearest neighbor of the former one) with atop CO can pop out of the surface, to form a newly-elevated species. In other words, we see a wave-like propagation of the Cu*CO adatoms across the surface.

Since the event is rather rare during regular MD, we perform slow-growth sampling (see Methods and Supplementary Note 4 for details) to obtain the free energy profile of the

propagation, with the height of the initial Cu*CO as the reaction coordinate. As the initial Cu*CO gets pressed back into the top surface layer, another surface Cu with atop CO in the second coordination sphere pops up, effectively propagating the Cu*CO over the surface. The barrier of this indirect diffusion process is as low as 0.10 eV, which is feasible at room temperature and is expected to be the major migration pathway of the elevated Cu*CO, rather than direct diffusion. The little kinetic hinderance of this process likely originates in the dynamics of adjacent H adsorbates that accompanies the Cu*CO propagation. To be specific, among the three H adsorbates that directly bond to the initially-elevated Cu*CO, the H closest to the later-elevated Cu*CO diffuses towards, and eventually binds to, the latter, breaking away from the initially-elevated Cu*CO as it sinks back into the top surface (Figure S7a). In the meantime, the H farthest from the later-elevated Cu*CO also breaks off and diffuses in the opposite direction, away from the initially-elevated Cu*CO, and stabilizes itself at a three-fold hollow site. Both initially- and newly-elevated Cu*CO share a similar coordination environment, binding to three H adsorbates below that are supported on a pentagonal local arrangement of surface Cu (Figure S7b-c). The diffusion of H adsorbate configurations is an indispensable part of the propagation process, as the local arrangement of the H determines the free energy landscape of Cu*CO (not a simple barrier-lowering effect), in a highly coupled manner.

When the elevated Cu*CO diffuses over the surface, it would eventually run into other elevated Cu*CO, and possibly seed an island formation. Hence, we further calculate the free energy profile of two Cu*CO interacting with each other, with the inter-Cu distance as the reaction coordinate. The obtained mechanism involves one of the Cu*CO rising from its initial adatom site and hop to a neighboring hollow site, in order to get closer to the other Cu*CO and dimerize (Figure 6). In the end, the two Cu*CO form an OC*Cu-Cu*CO dimer. This process has a significantly higher barrier of 0.36 eV, due to the need for one Cu*CO to break away from its initial surface site. As a result,

dimerization is expected to be much less frequent than diffusion, but the barrier should still be crossable at room temperature. The dimerization is also facilitated by local H arrangements (Figure S8): the H adsorbate in between the two Cu*CO's firstly hops from the initial site to a metastable out-of-plane bridge site, so that it can attract and coordinate to both Cu*CO's, to draw them closer to each other. As the two Cu*CO's get close enough and dimerize, the in-between H sinks back to a distorted hollow site and act as a supporting ligand from below, shared by both Cu atoms in the OC*Cu-Cu*CO dimer. This could be the underlying mechanism of Cu clustering and island formation on Cu electrodes in CO_2RR conditions.

CONCLUSIONS

In this work, we extensively explore the chemical space of Cu surface restructuring under mixed coverage of H and CO using a grand canonical global optimization technique, and construct the grand canonical ensemble representation of the surface in electrochemical conditions. The surface is predicted to significantly roughen under intermediate coverages of both H and CO, however, the potential dependence of the restructuring is not well described by Boltzmann statistics, as the system is non-equilibrium. A quasi-kinetic Monte Carlo method is developed to simulate the evolution of the surface under varying reducing potentials, with kinetic trapping considered. The "path" of the system across the metastable regime is identified, as well as the accessible reconstructed structures along the way. Under intermediate coverages of both H and CO, elevated Cu*CO species can emerge, which are lifted above the top surface by about 1 Å and not "adatoms" in a strict sense and creates no immediate vacancies. Chemical bonding analysis reveals the origin of the elevated Cu*CO species to be the combined effects of surface Cu-Cu bond weakening by H and atop coordination of the strong ligand CO. Molecular dynamics simulation and free energy calculations are performed to investigate the further evolution of the Cu*CO species. We found that it can readily diffuse over the surface via a novel propagation mechanism where one Cu*CO sinks back into the top surface and another Cu*CO unit pops up, creating a standing wave. Two Cu*CO may also dimerize with a slightly higher barrier, which is likely the underlying mechanism of further clustering and island formation. This work provides atomic insight into the roughening behaviour of Cu electrocatalysts and a way to address complex restructurings that are induced by coverage of mixed adsorbates and far from equilibrium. The overall high surface dynamism, with fascicle propagation of Cu*CO in the presence of H, raises a question of relevant active site(s) for CO_2RR, which could form transiently in the process.

METHODS

1. Model Set-up

The Cu(100) surface is modeled by a 4-layer 6×6 supercell of Cu(100) termination with a cell dimension of 15.336 Å×15.336 Å (constructed with experimental lattice parameter from ref [18]). The bottom two layers of the slab are constrained as bulk region, and everything else is allowed to relax as the interface region. A vacuum slab of 15 Å thickness is added in Z direction to avoid spurious interactions between periodic images.

2. DFT calculations

The local optimizations and energy evaluation are performed with the RPBE functional[19] and PBE_PAW pseudopotentials[20] using the VASP program (version 5.4.4).[21–24] The convergence criteria for electronic and force minimization are set to 10^{-5} eV and 0.05 eV/Å during the global optimization and 10^{-6} eV and 0.01 eV/Å for the final refinement. Due to the relatively large system and sampling size, only the Γ *k*-point is sampled in the reciprocal space of the Brillouin zone throughout, and the cutoff energy for the kinetic energy of the plane-waves was 400 eV.

The transition states (TS) are located using climbing image nudged elastic band (CI-NEB) method[25] with image dependent pair potential (IDPP) interpolation.[26] Each TS geometry has been confirmed to have only one imaginary mode.

All electronic structure analyses are performed based on converged charge density or wavefunction. The Bader charges are calculated using Bader Charge Analysis program.[27] The QTAIM analysis is performed using the critic2 program using the Wigner-Seitz method with a subdivision level of 2.[28]

3. Grand Canonical Genetic Algorithm

To sample the chemical space of both Cu restructuring and adsorbate (H and CO) coverage/configuration, we performed global optimization using the grand canonical genetic algorithm (GCGA) as implemented in our open-source GOCIA python package (https://github.com/zishengz/gocia), which now supports mixed and polyatomic adsorbates. To be specific, the system is treated as a grand canonical ensemble of H and CO adsorbates, and the search target is to minimize the coverage-dependent grand canonical free energy Ω_{ads}:

$$\Omega_{\mathrm{ads}} = U - TS - \sum \mu_i N_i \approx E^{\mathrm{slab}-n\mathrm{H}} - E^{\mathrm{slab}} - n_{\mathrm{H}} \cdot \mu_{\mathrm{H}}(\mathrm{pH}, U, T) - n_{\mathrm{CO}} \cdot \mu_{\mathrm{CO}}(p_{\mathrm{CO}}, T) \quad (1)$$

Where the $E^{\mathrm{slab}-n\mathrm{H}}$ and E^{slab} are electronic energies of the adsorbate-covered and the bare Cu(100) slab. The vibrational contributions to free energy by the slab atoms are neglected considering their small contribution and high computational cost.[29] The chemical potential of H and of CO, μ_{H} and μ_{CO}, are calculated by:

$$\mu_{\mathrm{H}}(\mathrm{pH}, U, T) = \frac{1}{2} E_{\mathrm{H_2}}^{\mathrm{gas}} - \ln(10)\, k_{\mathrm{B}} T \mathrm{pH} - |e| U_{\mathrm{SHE}} + \left(\mathrm{ZPE}^{\mathrm{gas}} + C_p^{\mathrm{gas}} - TS^{\mathrm{gas}}\right) - \left(\mathrm{ZPE}^{\mathrm{ads}} + C_p^{\mathrm{ads}} - TS^{\mathrm{ads}}\right) \quad (2)$$

$$\mu_{\mathrm{CO}}(p_{\mathrm{CO}}, T) = \frac{1}{2} E_{\mathrm{CO}}^{\mathrm{gas}} + k_B T \ln \frac{p_{\mathrm{CO}}}{p^0} + \left(\mathrm{ZPE}^{\mathrm{gas}} + C_p^{\mathrm{gas}} - TS^{\mathrm{gas}}\right) - \left(\mathrm{ZPE}^{\mathrm{ads}} + C_p^{\mathrm{ads}} - TS^{\mathrm{ads}}\right) \quad (3)$$

Where the pH and U (in SHE scale) dependent terms are calculated using the computational hydrogen electrode model.[30] The ZPE and thermal contribution terms of adsorbates are obtained from frequency calculations and evaluated at 298.15 K.

A population size of 25 and a mutation rate of 30% are chosen for the GCGA sampling. The pool of initial candidates is generated using the bond length distribution algorithm (BLDA) which is a random structure generation method based on the covalent radii of the atoms.[31] A pre-optimization with Hookean potential is performed to produce reasonable starting geometries before they are fed to electronic structure codes for local optimization and energy evaluation. Mating between the alive candidates to create offspring is done by the Split-and-splice operation,[32] in which the parent slabs are cut along a random plane and then spliced together. Fitness factor is assigned to each

candidate based on the mating counts and the grand canonical free energy. Candidates with higher fitness (low free energy) are more probable to mate. Similarity check against the current population is performed before adding any new candidate, to remove duplicates. Adopted mutation operations include: (1) adding or removing an adsorbate, (2) rattling the surface atoms along random vectors drawn from a normal distribution, (3) translating the buffer slab along x or y axis by 1/n (n=2,3,6) of the cell length, (4) permuting a random half of buffer region (original slab and the sampled adsorbates). If an offspring is too similar to its parent, its mutation rate is raised to 100%. Upon the addition of each offspring to the population, the candidate with the lowest fitness is archived to maintain the population size. The structures with unbound fragments are removed from the population to avoid sampling into chemically irrelevant regions of the PES.

4. Grand canonical DFT calculations.

For the lowest structures in the obtained ensembles, the electrochemical conditions beyond CHE are applied. Under a constant applied potential, the electrode surface is effectively a grand canonical ensemble of electrons where the number of electrons is varied to adapt to the change in the workfunction of the surface. The potential-dependent electronic grand canonical free energy of the surface Ω_{el} can be approximated by a surface charging model:[33]

$$\Omega_{\mathrm{el}}(U) = E(U) - q(U) \cdot FU \approx E(U_0) - \frac{1}{2} C (U - U_0)^2 \qquad (4)$$

Which treats the electrochemical interface as an effective capacitor. Here, $E(U)$ is the electronic energy of the surface under a potential U which is calculated by refencing the Fermi level of the system against the vacuum level. $q(U)$ is the surface charge difference referenced against the neutral system, and F is the Faradaic constant. U_0 stands for the potential of zero charge in vacuum scale, and C is the effective capacitance.

The self-consistent implicit solvation model VASPsol[34] is used to represent the polarizable electrolyte region. The surface slab is symmetrized along z axis to avoid asymmetric potential in the implicit solvation region. The thickness of implicit solvent slab is increased to 5λ where the Debye screening length is evaluated by:[35]

$$\lambda \approx \frac{3}{\sqrt{I}}\text{Å} \tag{5}$$

Where I is the ionic strength in M, in this study we take it to be 0.1 to model the 0.1 M $HClO_4$. Hence the implicit solvent thickness is set to 50 Å for the symmetrized slab (Figure S1c).

By varying the number of electrons in the system, the $E(U)$ of the system at the corresponding U and $q(U)$ can be obtained, and thereby a quadratic relation between $\Omega_{el}(U)$ and U can be fitted by sampling a series of q values (see Supplementary Note 2 for details). The U (in vacuum scale) can be converted into the SHE scale by referencing it against the benchmarked value (4.60 V for VASPsol).[36]

The final coverage- and potential-dependent grand canonical free energy Ω_{tot} is approximated by:

$$\Omega_{\text{tot}}(n, U) \approx \Omega_{\text{el}}^{\text{slab}-n\text{H}}(U) - \Omega_{\text{el}}^{\text{slab}}(U) - n \cdot \mu_{\text{H}}(\text{pH}, U, T) \tag{6}$$

5. Monte Carlo simulations.

The evolution of surface adsorbate coverage and configuration under varying potential is studied based on the structures in the ensemble and their potential-dependent free energies, from global optimization and grand canonical DFT calculations. The surface is modeled as a 10×10 lattice, with each grid representing a surface area of the size of the sampling cell.

During each simulation step, two types of moves can be made: (1) Intra-surface exchange, in which one random grid donates a random adsorbate to its neighboring grid;

(2) Surface-electrolyte exchange, in which one random grid gains or loses a random adsorbate. The end state of a grid after a move is a randomly selected minimum structure of its corresponding coverage state. The chemical potential of the adsorbate in the reservoir is constant and depends solely on the reaction conditions. The barrier associated with a move is assumed to scale with the change in free energy, which introduces a sense of kinetics into the simulation.

A move is accepted or rejected based on the Metropolis criteria. The temperature of the simulation is set to be 298.15 K, corresponding to room temperature conditions. The system is started at 0.25 V_{RHE} and then varied by 10 mV toward the negative voltage, every 2 million simulation steps. During each phase of the simulated cathodic scan, the system could not reach equilibrium but a quasi-equilibrium corresponding to a metastable regime at that potential. The simulation can hence track the evolution of the kinetically trapped system on a changing free energy landscape and locate its path across the configurational space.

Note that, although the absolute time factor associated with each move is lacking, the simulation should be able to reflect relative time scales at microsecond level. A rigorous kinetic Monte Carlo set up would require evaluation of free energy barrier of every possible move in the ensemble, and determination of pre-exponential factors for calculating the rates, which are prohibitively expensive and beyond the scope of this study.

6. Molecular dynamics.

The ab initio molecular dynamics simulations are performed on the optimized structures with the same DFT setting as the geometry optimization using the VASP program. The

simulation is performed in the NVT (canonical) ensemble at 300 K with the Nose-Hoover thermostat, with a time step of 1 fs.

The slow-growth technique is used to sample the free energy profiles. Specifically, the collective variable (reaction coordinate) corresponding to the studied process is varied very slowly during the sampling, so that all other variables are well equilibrated. The resulting trajectory constitutes a blue moon ensemble and can be used to calculate free energetics by thermodynamic integration. The height of the Cu atom in Cu*CO and the inter-Cu distance are used as the collective variable for the propagation and dimerization, respectively.

ASSOCIATED CONTENT

Supporting Information.

The following files are available free of charge at xxx.

Structural model for GCGA and GCDFT calculations; Statistics of vertical displacement of surface Cu atoms on other facet; Model set-up of the Monte Carlo simulation and the simulated cathodic scan; Evolution of the surface phases under varying potential from the statistics of the Monte Carlo simulation; Chemical bonding analysis of the elevated Cu*CO species; Model set-ups and details of the free energy calculations; Close-up views of the Cu*CO propagation and dimerization processes; Note on the modifications to the GCGA to support polyatomic adsorbates; Note on the details, related timescales, and limitations of the Monte Carlo simulation; Note on chemical bonding analysis of the H-promoted elevation of Cu*CO; Note on details and limitations of the slow-growth MD for free energy profile.

AUTHOR INFORMATION

Corresponding Author

*Corresponding Author's email:

Anastassia N. Alexandrova: ana@chem.ucla.edu

Philippe Sautet: sautet@ucla.edu

Notes

The authors declare no competing financial interest.

ACKNOWLEDGMENTS

The work was supported by the National Science Foundation CBET grant 2103116. Z.Z. was supported by the Dissertation Year Fellowship of UCLA. Computational resources for

this work were provided by UCLA shared cluster Hoffman2, and the Innovative and Novel Computational Impact on Theory and Experiment (INCITE) program at the Argonne Leadership Computing Facility, which is a DOE Office of Science User Facility supported under Contract DE-AC02-06CH11357.

REFERENCES

(1) Zhang, Z.; Zandkarimi, B.; Alexandrova, A. N. Ensembles of Metastable States Govern Heterogeneous Catalysis on Dynamic Interfaces. *Acc. Chem. Res.* 2020, *53* (2), 447–458. https://doi.org/10.1021/acs.accounts.9b00531.

(2) Lavroff, R. H.; Morgan, H. W. T.; Zhang, Z.; Poths, P.; Alexandrova, A. N. Ensemble Representation of Catalytic Interfaces: Soloists, Orchestras, and Everything in-Between. *Chem. Sci.* 2022, *13* (27), 8003–8016. https://doi.org/10.1039/d2sc01367c.

(3) Nitopi, S.; Bertheussen, E.; Scott, S. B.; Liu, X.; Engstfeld, A. K.; Horch, S.; Seger, B.; Stephens, I. E. L.; Chan, K.; Hahn, C.; Nørskov, J. K.; Jaramillo, T. F.; Chorkendorff, I. Progress and Perspectives of Electrochemical CO2 Reduction on Copper in Aqueous Electrolyte. *Chem. Rev.* 2019, *119* (12), 7610–7672. https://doi.org/10.1021/acs.chemrev.8b00705.

(4) Piqué, O.; Low, Q. H.; Handoko, A. D.; Yeo, B. S.; Calle-Vallejo, F. Selectivity Map for the Late Stages of CO and CO2 Reduction to C2 Species on Copper Electrodes. *Angew. Chemie Int. Ed.* 2021, *60* (19), 10784–10790. https://doi.org/https://doi.org/10.1002/anie.202014060.

(5) Dattila, F.; García-Muelas, R.; López, N. Active and Selective Ensembles in Oxide-Derived Copper Catalysts for CO2 Reduction. *ACS Energy Lett.* 2020, *5* (10), 3176–3184.

(6) Kim, Y. G.; Baricuatro, J. H.; Javier, A.; Gregoire, J. M.; Soriaga, M. P. The Evolution of the Polycrystalline Copper Surface, First to Cu(111) and Then to Cu(100), at a Fixed CO2RR Potential: A Study by Operando EC-STM. *Langmuir* 2014, *30* (50), 15053–15056. https://doi.org/10.1021/la504445g.

(7) Huang, J.; Hörmann, N.; Oveisi, E.; Loiudice, A.; De Gregorio, G. L.; Andreussi, O.; Marzari, N.; Buonsanti, R. Potential-Induced Nanoclustering of Metallic

Catalysts during Electrochemical CO2 Reduction. *Nat. Commun.* 2018, *9* (1), 3117. https://doi.org/10.1038/s41467-018-05544-3.

(8) Eren, B.; Zherebetskyy, D.; Patera, L. L.; Wu, C. H.; Bluhm, H.; Africh, C.; Wang, L. W.; Somorjai, G. A.; Salmeron, M. Activation of Cu(111) Surface by Decomposition into Nanoclusters Driven by CO Adsorption. *Science.* 2016, *351* (6272), 475–478. https://doi.org/10.1126/science.aad8868.

(9) Auer, A.; Andersen, M.; Wernig, E. M.; Hörmann, N. G.; Buller, N.; Reuter, K.; Kunze-Liebhäuser, J. Self-Activation of Copper Electrodes during CO Electro-Oxidation in Alkaline Electrolyte. *Nat. Catal.* 2020, *3* (10), 797–803. https://doi.org/10.1038/s41929-020-00505-w.

(10) Amirbeigiarab, R.; Tian, J.; Herzog, A.; Qiu, C.; Bergmann, A.; Roldan Cuenya, B.; Magnussen, O. M. Atomic-Scale Surface Restructuring of Copper Electrodes under CO2 Electroreduction Conditions. *Nat. Catal.* 2023, *6* (9), 837–846. https://doi.org/10.1038/s41929-023-01009-z.

(11) Wan, M.; Yang, Z.; Morgan, H.; Shi, J.; Shi, F.; Liu, M.; Wong, H.-W.; Gu, Z.; Che, F. Enhanced CO2 Reactive Capture and Conversion Using Aminothiolate Ligand–Metal Interface. *J. Am. Chem. Soc.* 2023, *145* (48), 26038–26051. https://doi.org/10.1021/jacs.3c06888.

(12) Ummireddi, A. K.; Li, Z.; Wu, J. Copper Defects for CO2 Electrocatalysis toward a Specific Multicarbon Product. *Trends Chem.* 2023.

(13) Zhang, Z.; Wei, Z.; Sautet, P.; Alexandrova, A. N. Hydrogen-Induced Restructuring of a Cu(100) Electrode in Electroreduction Conditions. *J. Am. Chem. Soc.* 2022, *144* (42), 19284–19293. https://doi.org/10.1021/jacs.2c06188.

(14) Cheng, D.; Wei, Z.; Zhang, Z.; Broekmann, P.; Alexandrova, A. N.; Sautet, P. Restructuring and Activation of Cu(111) under Electrocatalytic Reduction Conditions. *Angew. Chemie - Int. Ed.* 2023, *62* (20), e202218575.

https://doi.org/10.1002/anie.202218575.

(15) Wan, C.; Zhang, Z.; Dong, J.; Xu, M.; Pu, H.; Baumann, D.; Lin, Z.; Wang, S.; Huang, J.; Shah, A. H.; Pan, X.; Hu, T.; Alexandrova, A. N.; Huang, Y.; Duan, X. Amorphous Nickel Hydroxide Shell Tailors Local Chemical Environment on Platinum Surface for Alkaline Hydrogen Evolution Reaction. *Nat. Mater.* 2023, *22* (8), 1022–1029. https://doi.org/10.1038/s41563-023-01584-3.

(16) Zhang, Z.; Hermans, I.; Alexandrova, A. N. Off-Stoichiometric Restructuring and Sliding Dynamics of Hexagonal Boron Nitride Edges in Conditions of Oxidative Dehydrogenation of Propane. *J. Am. Chem. Soc.* 2023, *145* (31), 17265–17273. https://doi.org/10.1021/jacs.3c04613.

(17) Zhang, Z.; Masubuchi, T.; Sautet, P.; Anderson, S. L.; Alexandrova, A. N. Hydrogen Evolution on Electrode-Supported Ptn Clusters: Ensemble of Hydride States Governs the Size Dependent Reactivity. *Angew. Chemie - Int. Ed.* 2023, *62* (20), e202218210. https://doi.org/10.1002/anie.202218210.

(18) Janthon, P.; Luo, S.; Kozlov, S. M.; Viñes, F.; Limtrakul, J.; Truhlar, D. G.; Illas, F. Bulk Properties of Transition Metals: A Challenge for the Design of Universal Density Functionals. *J. Chem. Theory Comput.* 2014, *10* (9), 3832–3839. https://doi.org/10.1021/ct500532v.

(19) Hammer, B.; Hansen, L. B.; Nørskov, J. K. Improved Adsorption Energetics within Density-Functional Theory Using Revised Perdew-Burke-Ernzerhof Functionals. *Phys. Rev. B - Condens. Matter Mater. Phys.* 1999, *59* (11), 7413–7421. https://doi.org/10.1103/PhysRevB.59.7413.

(20) Joubert, D. From Ultrasoft Pseudopotentials to the Projector Augmented-Wave Method. *Phys. Rev. B - Condens. Matter Mater. Phys.* 1999, *59* (3), 1758–1775. https://doi.org/10.1103/PhysRevB.59.1758.

(21) Kresse, G.; Furthmüller, J. Efficiency of Ab-Initio Total Energy Calculations for

Metals and Semiconductors Using a Plane-Wave Basis Set. *Comput. Mater. Sci.* 1996, *6* (1), 15–50. https://doi.org/10.1016/0927-0256(96)00008-0.

(22) Kresse, G.; Furthmüller, J. Efficient Iterative Schemes for Ab Initio Total-Energy Calculations Using a Plane-Wave Basis Set. *Phys. Rev. B - Condens. Matter Mater. Phys.* 1996, *54* (16), 11169–11186. https://doi.org/10.1103/PhysRevB.54.11169.

(23) Kresse, G. Ab Initio Molecular Dynamics for Liquid Metals. *J. Non. Cryst. Solids* 1995, *192–193* (1), 222–229. https://doi.org/10.1016/0022-3093(95)00355-X.

(24) Kresse, G.; Hafner, J. Ab Initio Molecular-Dynamics Simulation of the Liquid-Metalamorphous- Semiconductor Transition in Germanium. *Phys. Rev. B* 1994, *49* (20), 14251–14269. https://doi.org/10.1103/PhysRevB.49.14251.

(25) Henkelman, G.; Uberuaga, B. P.; Jónsson, H. Climbing Image Nudged Elastic Band Method for Finding Saddle Points and Minimum Energy Paths. *J. Chem. Phys.* 2000, *113* (22), 9901–9904. https://doi.org/10.1063/1.1329672.

(26) Smidstrup, S.; Pedersen, A.; Stokbro, K.; Jónsson, H. Improved Initial Guess for Minimum Energy Path Calculations. *J. Chem. Phys.* 2014, *140* (21), 214106. https://doi.org/10.1063/1.4878664.

(27) Yu, M.; Trinkle, D. R. Accurate and Efficient Algorithm for Bader Charge Integration. *J. Chem. Phys.* 2011, *134* (6), 64111. https://doi.org/10.1063/1.3553716.

(28) Otero-De-La-Roza, A.; Johnson, E. R.; Luaña, V. Critic2: A Program for Real-Space Analysis of Quantum Chemical Interactions in Solids. *Comput. Phys. Commun.* 2014, *185* (3), 1007–1018. https://doi.org/10.1016/j.cpc.2013.10.026.

(29) Sun, G.; Alexandrova, A. N.; Sautet, P. Structural Rearrangements of Subnanometer Cu Oxide Clusters Govern Catalytic Oxidation. *ACS Catal.* 2020, *10* (9), 5309–5317. https://doi.org/10.1021/acscatal.0c00824.

(30) Yang, T. T.; Patil, R. B.; McKone, J. R.; Saidi, W. A. Revisiting Trends in the Exchange Current for Hydrogen Evolution. *Catal. Sci. Technol.* 2021, *11* (20), 6832–6838. https://doi.org/10.1039/d1cy01170g.

(31) Zhai, H.; Alexandrova, A. N. Ensemble-Average Representation of Pt Clusters in Conditions of Catalysis Accessed through GPU Accelerated Deep Neural Network Fitting Global Optimization. *J. Chem. Theory Comput.* 2016, *12* (12), 6213–6226. https://doi.org/10.1021/acs.jctc.6b00994.

(32) Deaven, D. M.; Ho, K. M. Molecular Geometry Optimization with a Genetic Algorithm. *Phys. Rev. Lett.* 1995, *75* (2), 288–291. https://doi.org/10.1103/PhysRevLett.75.288.

(33) Steinmann, S. N.; Michel, C.; Schwiedernoch, R.; Sautet, P. Impacts of Electrode Potentials and Solvents on the Electroreduction of CO2: A Comparison of Theoretical Approaches. *Phys. Chem. Chem. Phys.* 2015, *17* (21), 13949–13963. https://doi.org/10.1039/c5cp00946d.

(34) Mathew, K.; Sundararaman, R.; Letchworth-Weaver, K.; Arias, T. A.; Hennig, R. G. Implicit Solvation Model for Density-Functional Study of Nanocrystal Surfaces and Reaction Pathways. *J. Chem. Phys.* 2014, *140* (8), 84106. https://doi.org/10.1063/1.4865107.

(35) Steinmann, S. N.; Sautet, P. Assessing a First-Principles Model of an Electrochemical Interface by Comparison with Experiment. *J. Phys. Chem. C* 2016, *120* (10), 5619–5623. https://doi.org/10.1021/acs.jpcc.6b01938.

(36) Mathew, K.; Kolluru, V. S. C.; Mula, S.; Steinmann, S. N.; Hennig, R. G. Implicit Self-Consistent Electrolyte Model in Plane-Wave Density-Functional Theory. *J. Chem. Phys.* 2019, *151* (23), 234101. https://doi.org/10.1063/1.5132354.